RSC Advances

PAPER

View Article Online
View Journal | View Issue

Cite this: *RSC Adv.*, 2023, **13**, 34817

Palladium-anchored donor-flexible pyridylidene amide (PYA) electrocatalysts for CO_2 reduction†

Afshan Khurshid, ‡[a] Tania Tanveer,‡[a] Komal Hafeez,‡[a] Maqsood Ahmed, [b] Zareen Akhtar[a] and M. Naveed Zafar *[a]

Received 22nd September 2023
Accepted 15th November 2023

DOI: 10.1039/d3ra06477h

rsc.li/rsc-advances

The conversion of CO_2 into CO as a substitute for processing fossil fuels to produce hydrocarbons is a sustainable, carbon neutral energy technology. However, the electrochemical reduction of CO_2 into a synthesis gas (CO and H_2) at a commercial scale requires an efficient electrocatalyst. In this perspective, a series of six new palladium complexes with the general formula [Pd(L)(Y)]Y, where L is a donor-flexible PYA, N^2,N^6-bis(1-ethylpyridin-4(1*H*)-ylidene)pyridine-2,6-dicarboxamide, N^2,N^6-bis(1-butylpyridin-4(1*H*)-ylidene)pyridine-2,6-dicarboxamide, or N^2,N^6-bis(1-benzylpyridin-4(1*H*)-ylidene) pyridine-2,6-dicarboxamide, and Y = OAc or Cl^-, were utilized as active electrocatalysts for the conversion of CO_2 into a synthesis gas. These palladium(II) pincer complexes were synthesized from their respective H-PYA proligands using 1,8-diazobicyclo[5.4.0]undec-7-ene (DBU) or sodium acetate as a base. All the compounds were successfully characterized by various physical methods of analysis, such as proton and carbon NMR, FTIR, CHN, and single-crystal XRD. The redox chemistry of palladium complexes toward carbon dioxide activation suggested an evident CO_2 interaction with each Pd(II) catalyst. [Pd(N^2,N^6-bis(1-ethylpyridin-4(1*H*)-ylidene)pyridine-2,6-dicarboxamide)(Cl)]Cl showed the best electrocatalytic activity for CO_2 reduction into a synthesis gas under the acidic condition of trifluoracetic acid (TFA) with a minimum overpotential of 0.40 V, a maximum turnover frequency (TOF) of 101 s^{-1}, and 58% FE of CO. This pincer scaffold could be stereochemically tuned with the exploration of earth abundant first row transition metals for further improvements in the CO_2 reduction chemistry.

1 Introduction

Carbon dioxide emissions are gradually increasing due to natural and anthropogenic activities, thus leading to global warming. The reduction of carbon dioxide to carbon neutral, valuable products is of major interest for researchers to overcome global warming challenges and energy deficiencies.[1] An easier alternative to complex, less efficient catalytic processes involving the direct conversion of CO_2 into hydrocarbons is the electrochemical conversion of CO_2 into a synthesis gas (CO and H_2), followed by the Fisher Tropsch reaction. The two-electron reduction of CO_2 to CO (eqn (1)) is also beneficial, since CO is used as a precursor in numerous industrial processes.[2] In this instance, however, a rival reaction (eqn (2)) is the direct proton reduction into hydrogen.

$$CO_2 + 2H^+ + 2e^- \rightarrow CO + H_2O,\ E^0 = -0.77\ \text{V}\ \textit{vs.}\ \text{SCE} \quad (1)$$

$$2H^+ + 2e^- \rightarrow H_2,\ E^0 = -0.66\ \text{V}\ \textit{vs.}\ \text{SCE} \quad (2)$$

Many scientists across the globe have worked on the CO_2 reduction into CO utilising homogeneous electrocatalysts with the aim to achieve a high activity and selectivity. Following the earlier discovery of a Rh-phosphine electrocatalyst by Wagenknecht *et al.* in 1984,[3] DuBois and co-workers[4–8] focused almost solely on the development of pincer Pd-phosphine based homogeneous electrocatalysts of the type $[Pd(L_3)(CH_3CN)](BF_4)_2$ for the CO_2-reduction reaction (CRR). They detected CO gas as a major reduction product under acidic conditions in both dimethylformamide (DMF) and acetonitrile (CH_3CN) solvents.[5] DuBois also proposed the reaction mechanism for the palladium-catalyzed conversion of CO_2 to CO. The rate-determining step was demonstrated by the addition of a high acid concentration that led to the η^1-C model of CO_2. A few examples of homogeneous palladium complexes were reported by Ogura for the CRR with nitrogen donor ligands, such as pyridine, pyrazole,[9] quinoline, bipyridine, and phenanthroline.[10]

[a]*Department of Chemistry, Quaid-i-Azam University, Islamabad, 45320, Pakistan. E-mail: mnzafar@qau.edu.pk*

[b]*Materials Chemistry Laboratory, Department of Chemistry, The Islamia University of Bahawalpur, 63100, Pakistan*

† Electronic supplementary information (ESI) available: Spectroscopic data of all compounds **1–11** (S1–S11), crystal data of **2**, **4**, **11** (S12 and S13) and cyclic voltammograms of **6–11** under different conditions (S13 and S14) are in ESI. CCDC 2281737–2281739. For ESI and crystallographic data in CIF or other electronic format see DOI: https://doi.org/10.1039/d3ra06477h

‡ Authors contributed equally to this manuscript.

Pincer complexes are of particular interest in the field of redox catalysis owing to their strong chelating effect, preorganized geometry, high tunability, and potential for ligand-based redox activity.[11–13] Several pincer complexes have been described in literature for the electrocatalytic CO_2 reduction reaction (CRR) as shown in Fig. 1.[14–24] Some early examples include Abruna's catalyst; with which bis(imino)pyridine anchored cobalt[14,15] yielded formic acid as a reduced CRR product. Kang *et al.* created a similar pincer ligand but one imino arm was replaced with rigid pyridine to access a bipyridyl unit that increased the selectivity of cobalt for formate.[16] Fontecave made a more selective cobalt terpyridine-based electrocatalyst for the reduction of CO_2 to CO.[17,18] Jurss and co-workers created a bipyridyl phosphine based mixed-donor ligand and achieved CO_2 reduction catalysis at lower potentials.[19] Richeson's PNP-ligated manganese–tricarbonyl complex achieved the conversion of CO_2 to CO without the use of an additional Brønsted acid.[20] Several studies by Hollis, Sun, and Luca on a C^C^C pincer based on N-heterocyclic carbene showed this supporting framework to be efficient for transition metal-based CO_2 reduction catalysis.[21–23] Similarly, Wolf developed a series of various C^N^C pincer palladium complexes with N-heterocyclic carbene for the CRC[24–28] and studied the effect of various substitutions on the ligand architecture as well as metal replacement on the CRC. His work concluded that conjugated NHC catalysts with palladium worked much better for the CRR than Ni and Pt analogues. Although these palladium complexes were electrolytically stable and showed current augmentation under CO_2, the faradaic efficiency (FE) for CO generation remained below 50%.

Here in this study, we aimed to utilize the potential of the donor-flexible and pincer-shaped pyridylidene amide (PYA) ligands toward palladium-catalyzed CO_2 reduction into synthesis gas. In this regard, a series of new pyridylidene amide (PYA) proligands and their respective palladium complexes were synthesized and successfully characterized with various spectroscopic techniques and single-crystal XRD. The PYA ligand existed in two major limiting resonating forms (Fig. 2) and could tune the electron donation to the metal according to the requirement during catalytic cycles (Fig. 2).[29–32] The resonance adaptation, inductive effect of various substituents on the PYA spectator ligand, and effect of different labile ligands (OAc, Cl) were investigated for palladium-centered CO_2 activation.

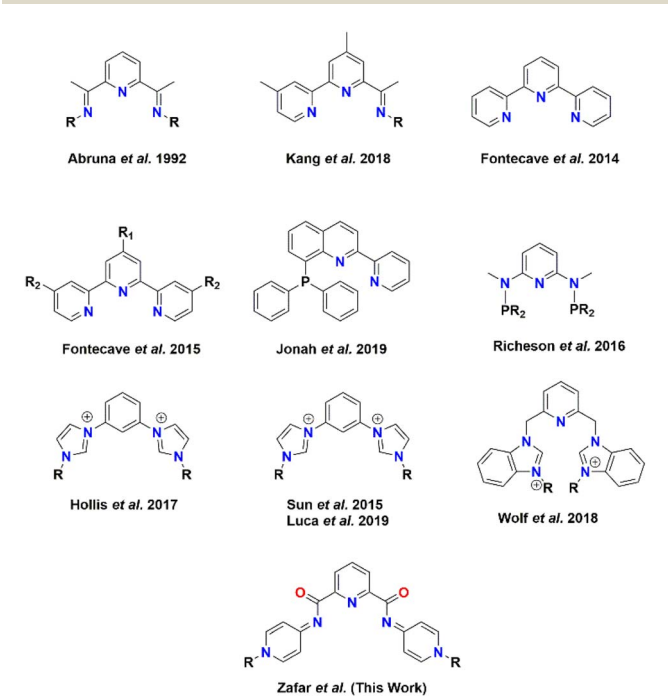

Fig. 1 Some selected pincer spectator ligands for the transition metal-catalyzed CO_2 electroreduction.

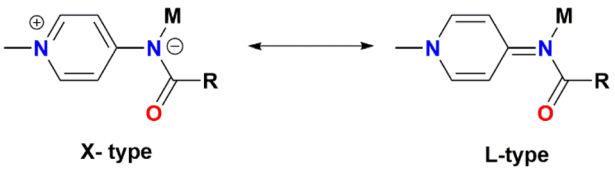

Fig. 2 The limiting resonance forms of PYA.

2 Results and discussion

2.1 Synthesis and characterization of proligands (1–4)

Precursor (**1**) was synthesized from 4-aminopyridine and pyridine-2,6-dicarbonyldichloride from a previously reported method.[33] The further alkylation of **1** was carried out using various alkylating reagents, such as ethyl iodide, butyl bromide, and benzyl chloride, in acetonitrile that afforded the proligands H-PYAs (**2–4**) (Scheme 1).

The H-PYAs were characterized using different spectroscopic and structural techniques, like ^{1}H NMR, ^{13}C NMR, FTIR, and X-ray diffraction single-crystal analysis (S12†). The characterization data of **1** resembled the reported values.[33] The representative ^{1}H and ^{13}C NMR of the **2–5** are given in Table 1. The proton NMR of the proligands showed NH peaks in the range of 13.19–11.27 ppm and aromatic peaks from 7.41 to 9.06 ppm. There were no aliphatic protons in **1** while **2–5** showed the aliphatic protons in the usual aliphatic region from 5.77–1.38 ppm. The C=O peak was observed from 163.3–170.7 ppm when analyzed by ^{13}C NMR. Aliphatic methylene carbon signals were observed in the range of 19.2–62.2 ppm while the methyl carbons were found between 13.8–16.5 ppm in the carbon NMR. In the FTIR spectra, N–H stretching band was noticed in the range of 3400–3482 cm^{-1}. The C=O, aromatic C–H, aliphatic C–H, and C=N stretching bands were found in the ranges of 1645–1694, 3032–3098, 2900–2998, and 1556–1652 cm^{-1}, respectively.[34]

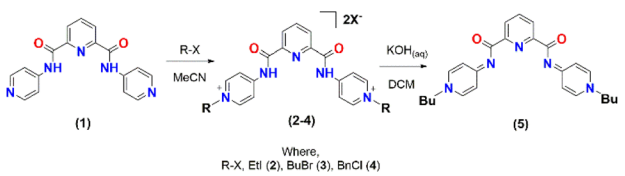

Scheme 1 The synthesis of proligands (**2–4**) and ligand (**5**) from (**1**).

Table 1 Representative ^{1}H and ^{13}C NMR δ (ppm) of **2–5** in DMSO-d_6

Compounds	**2**		**3**		**4**		**5**	
Protons/carbons	δ_H	δ_C	δ_H	δ_C	δ_H	δ_C	δ_H	δ_C
NH	11.97	—	12.19	—	13.29	—	—	—
Ar–H/C	9.02–8.59	151.5–116.7	9.07–8.56	151.7–116.8	9.14–7.54	152.9–117.4	8.77–7.94	161.5–125.8
CO	—	163.7	—	164.0	—	164.6	—	170.5
CH_2 (α)	4.59	55.4	4.54	59.5	5.77	62.2	4.55	59.2
CH_2 (β)	—	—	—	32.9	—	—	1.89	32.9
CH_2 (Υ)	—	—	—	19.2	—	—	1.32	19.2
CH_3	1.58	16.5	1.90	13.8	—	—	0.94	13.8

2.2 Synthesis and characterization of palladium(II) complexes (6–11)

Palladium complexes with different proligands (H-PYAs) were synthesized by *in situ* deprotonations of H-PYAs (**2–4**) with 1,8-diazobicyclo[5.4.0]undec-7-ene (DBU) (in **2** and **4**) or sodium acetate (in case of **3**). The ligands generated with the help of weak base were treated with palladium source *i–e* palladium acetate for **6–8** and bisbenzonitrilepalladium(II) chloride for **9–11**. The synthetic protocol is summarized in Scheme 2.

The palladium complexes were well characterized using various spectroscopic and structural techniques, like ^{1}H NMR, ^{13}C NMR, FTIR, and X-ray diffraction single-crystal analysis (S13†). The representative ^{1}H and ^{13}C NMR of the **6–11** are given in Table 2. The absence of the NH peak in **6–11** was confirmed by proton NMR. All the aromatic peaks were shifted to a more shielded region due to the resonance of amidate electrons on the whole complex in both proton and carbon NMR. The acetate ligand was revealed in **6–8** as a singlet for methyl that appeared in the range of 1.50–1.61 ppm. The C=O peaks in ^{13}C NMR were observed in the range of 162.1–170.7 ppm in all complexes, while the acetate carbonyl peaks in **6–8** appeared between 170.3–175.8 ppm. The appearance of these new peaks revealed the synthesis of these complexes. The aliphatic protons and carbons appeared in the normal range but were slightly shifted compared to the proligands. The absence of N–H band in the IR spectra supported the NMR results. The carbonyl bands of amidate and acetate appeared in their characteristic range of 1612–1658 cm^{-1} in the FTIR analysis.[34] The Pd–N bands for the complexes were observed in the range of 511–528 cm^{-1}.[35]

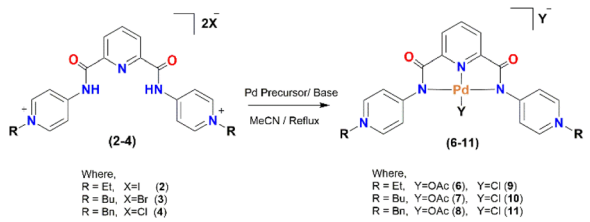

Scheme 2 The synthesis of palladium complexes (**6–11**) from proligands (**2–4**) using $Pd(OAc)_2$ or $Pd(PhCN)_2Cl_2$ as the palladium precursor and sodium acetate or DBU as the base.

Attempts were made to isolate all the ligands that were produced *in situ* during the complex formation reactions. However, only **5** was obtained as a white powder by the deprotonation of **3** with an aqueous solution of KOH followed by its extraction in dichloromethane (Scheme 1). The disappearance of the proligand amide N–H peak was observed both in the proton NMR (Table 1) and FTIR. A comparison of **5** with **7** and **10** showed that the protons and carbon signals were slightly shifted after complex formation.

2.3 Electrochemical behavior of palladium complexes (6–11) under N_2

To evaluate the redox behavior of the palladium complexes, cyclic voltammetry (CV) experiments were performed under an

Table 2 Representative ^{1}H and ^{13}C NMR δ (ppm) of **6–11** in DMSO-d_6

Compounds	**6**		**7**		**8**		**9**		**10**		**11**	
Protons/carbons	δ_H	δ_C	δ_H	δ_C	δ_H	δ_C	δ_H	δ_C	δ_H	δ_C	δ_H	δ_C
OAc (CO)	1.62	175.8	1.59	170.4	1.50	170.3	—	—	—	—	—	—
CO	—	170.3	—	162.0	—	162.1	—	170.5	—	170.5	—	170.5
Ar–H/C	8.75–7.89	161.7–123.0	8.78–7.90	149.4–126.6	8.90–7.47	149.4–123.2	8.76–7.95	161.5–125.7	8.77–7.94	161.5–125.7	8.90–7.53	161.8–125.9
OAc (CH_3)	—	24.8	—	19.2	—	24.7	—	—	—	—	—	—
CH_2 (α)	4.46	54.8	4.44 1.85 1.28	59.3	5.67	61.8	4.46	55.0	4.43 1.86 1.28	59.2	5.68	62.0
CH_2 (β)	—	—		32.9	—	—	—	—		32.9	—	—
CH_2 (Υ)	—	—		19.2	—	—	—	—		19.2	—	—
CH_3	1.51	16.6	0.93	13.8	—	—	1.53	16.5	0.91	13.8	—	—

inert atmosphere of nitrogen. The cyclic voltammograms of **6–11** under N_2 are represented as black line in Fig. 3, and some important parameters from the CV tests are given in Table 3. An H-cell with 2 mM solution of the catalyst in DMF and 0.1 M supporting electrolyte tetrabutylammonium hexafluorophosphate ($TBAPF_6$) was used in all the measurements. The appearance of anodic and cathodic peaks represented the redox active natures of **6–11**. An anodic peak for **6–8** emerged for the acetate and appeared from 0.5 V to 0.6 V, while the peaks observed at 0.3, −1.3, and −0.25 V could be related to complex oxidation. Similarly, **9–11** showed complex oxidation at 0.3, 0, and −0.2 V, respectively. Similarly, the halide oxidation occurred at 0.7, 0.8, and 0.3 V, respectively. Two to three irreversible cathodic waves appeared for all complexes (black line in Fig. 3), which could be attributed to the formation of redox species.[26] The first cathodic wave, E_{pc1}, for **6–11** ranged from −0.80 V to −0.98 V with peak current values, I_{pc1} in the range of 25 μA to 150 μA. The second cathodic wave, E_{pc2}, for the complexes appeared in the range of −1.33 V to −1.95 V with peak current values, I_{pc2}, ranging from 35 μA to 175 μA. The third cathodic events appeared at −1.80 V to −2.20 V with I_{pc3} values up to 160 μA for the palladium complexes. The cathodic waves could be related to the reduction of Pd(II) to Pd(I) and Pd(I) to Pd(0). The current under each peak increased with the increase in the scan rate according to Randles–Sevcik eqn (S15).†[36]

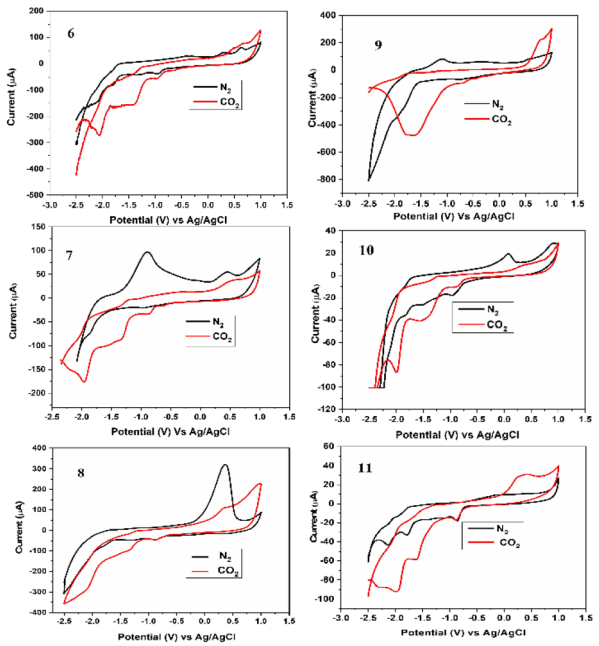

Fig. 3 The cyclic voltammograms of **6–11** under nitrogen (black line) and CO_2 (red line). All experiments were performed at 100 mV s^{-1} scan rate in DMF and 0.1 M supporting electrolyte ($TBAPF_6$).

Table 3 The CV features of **6–11** under N_2[a]

Catalysts	E_{pc1} (V)	E_{pc2} (V)	E_{pc3} (V)	E_{pa1} (V)	E_{pa2} (V)
6	−0.96	−1.80	−2.11	0.30	0.60
7	−0.80	−1.86	−1.82	−1.30	0.50
8	−0.87	−1.33	−1.80	−0.25	0.50
9	−0.70	−1.75	—	0.30	0.70
10	−0.98	−1.60	−1.89	—	0.80
11	−0.87	−1.95	−2.20	−0.20	0.30

[a] The peak potential of complexes **6–11** [2 mM] from CV measured at 100 mV s^{-1} in DMF containing 0.1 M ($TBAPF_6$) under N_2.

2.4 Electrochemical behavior of palladium complexes (6–11) under CO_2

To evaluate the electrochemical interactions of the palladium complexes with CO_2, cyclic voltammetry experiments were performed under a saturated environment of CO_2 by sparging the solution with carbon dioxide gas for 15 min before running the electrochemical reaction. The carbon dioxide bubbling in the electrolytic solution was done to not only ward-off all the reactive gases like oxygen from the solution but also to produce its reduced products. The cyclic voltammograms results under CO_2 and some important parameters are given in Fig. 3 (as red lines) and Table 4, respectively. Most of the cathodic peaks showed current enhancement, particularly **9** with peak current ratios of CO_2 to N_2 (I/I_{p0}) 1.41 at E_{pc1} and 2.58 at E_{pc2}. This was followed by complex **6** (acetate analogue of **9**), which indicated the optimized inductive synergistic effect of the ethyl groups on the palladium center *via* the pendant pyridinium rings of the spectator ligand for CO_2 activation. The chloride seemed a little better actor ligand compared to the acetate as complexes **9–11** showed a high cathodic peak current under the CO_2 environment compared to their respective acetate analogues (**6–8**). The complexes **7** and **10** with butyl pendent groups showed the least activity toward CO_2 activation followed by the benzylated complexes **8** and **11**. These current enhancements under the CO_2 environment compared to the inert gas suggested the formation of some CO_2 reduced products. The palladium complex with the ethylated pendant group on the spectator ligand and chloride as the actor ligand had a lower overpotential for CO_2 reduction than its acetate analogue. However, the palladium complex with the butyl substituent on the ligand and with acetate showed less overpotential compared to its chloride counterpart. However, the benzyl-bearing complex remained unaffected by the change of the labile ligand. The

Table 4 The CV features of **6–11** under CO_2[a]

Catalysts	E_{pc1}	ΔE_{pc1}	I/I_{p0}	E_{pc2}	ΔE_{pc2}	I/I_{p0}	E_{pc3}	ΔE_{pc3}
6	−0.94	−20	1.36	−1.47	330	2.00	−2.11	00
7	−0.81	−10	0.90	−1.38	480	1.33	−2.07	−250
8	−0.88	10	1.02	−1.34	−10	1.40	−2.12	−300
9	−0.68	20	1.41	−1.69	60	2.58	—	—
10	−0.92	60	0.54	−1.53	70	2.02	−1.99	−100
11	−0.88	−10	0.80	−1.63	320	2.51	−1.98	220

[a] Cathodic peak waves, change in potentials to N_2, and the peak current ratio of CO_2 to N_2 specified as i/i_{p0} of complexes **6–11**. CV data were collected at 100 mV s^{-1} in DMF with 2 mM complex and ($TBAPF_6$) as the supporting electrolyte.

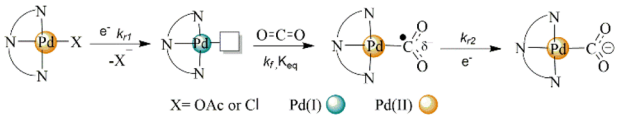

Scheme 3 The proposed mechanism for binding of the solvated CO_2 with the reduced pincer palladium catalyst.

palladium complex upon reduction released the actor ligand (acetate or chloride in this case) and interacted with the electrophilic carbon of CO_2 through its fourth coordination site (Scheme 3). The linear CO_2 molecule got bent upon its binding with the electron-rich palladium center.[24] The formation of [N^N^N–Pd(II)–COO•] was reflected by the enhancement in the cathodic peak currents in the cyclic voltammograms of the complexes under the saturated CO_2 environment (red lines, Fig. 3). This suggested the fastest and spontaneous interaction of CO_2 with **9** compared to other catalysts. A low current enhancement upon CO_2 interaction revealed the slowest kinetics for **7** and **10**. The magnitude of the homogeneous complexation (K (equilibrium constant) and k_f (rate constant)) or heterogeneous reduction (k_{r2} (rate constant)) demonstrated the peak position of E_{pc} (CO_2).[25] This in turn depended on the scan rate (timeframe of the experiment) relative to the scale of K and the rates of reduction. The shift of E_{pc} (CO_2) to a more negative potential revealed a larger value of K while a shift of E_{pc} (CO_2) to a less negative potential represented a larger k_{r2}.[37,38] Shifts in the position of E_{pc1} under CO_2 within the range of −10 mV to 60 mV were observed for all the complexes (Table 4). The maximum value of I_{pc1} (CO_2)/I_{pc1} (N_2) = 1.41, was observed at the first cathodic event for **9**. This represented the acceptance of a second electron by [N^N^N–Pd^{+2}COO•] species. Similarly, the reduction events at E_{pc2} (CO_2) showed a more positive potential compared to E_{pc2} (N_2) in almost all the complexes with large I_{pc2} (CO_2)/I_{pc2} (N_2) values up to 2.58 (in the case of **9**). This could be related to the larger value of K.[37,38]

2.5 Electrocatalysis of proton-promoted CO_2 reduction by palladium complex (9)

Complex **9** that showed the highest CO_2 activation (as mentioned above) was further studied under the reducing environment of protons. Different acids, such as glacial acetic acid (GAA), trifluoroethanol (TFE), and trifluoracetic acid (TFA), were utilized for this study. Complex **9** showed the best results with 10 mmol of TFA in terms of the cathodic current enhancements (blue line, Fig. 4A). Two distinct cathodic peaks, E_{pc1} and E_{pc2} at −1.04 and −1.95 V with peak currents I_{pc1} and I_{pc2} of 679 μA and 975 μA, respectively, were noticed. The current ratio of I_{cat}/I_p at E_{pc1} was 11.3 and at E_{pc2} was 8.2 for **9**. The maximum turnover frequency (TOF) of 101 s^{-1} and K_{cat} of 561 M^{-1} s^{-1} were obtained. The minimum overpotential obtained was 0.40 V for catalyst **9**. The TOF and k_{cat} were calculated by using eqn (3) from the literature.[39]

$$\mathrm{TOF} = K_{cat}[\mathrm{Q}] = \frac{Fvn_p{}^3}{RT}\left(\frac{0.4463}{n_{cat}}\right)^2\left(\frac{i_{cat}}{i_p}\right)^2 \quad (3)$$

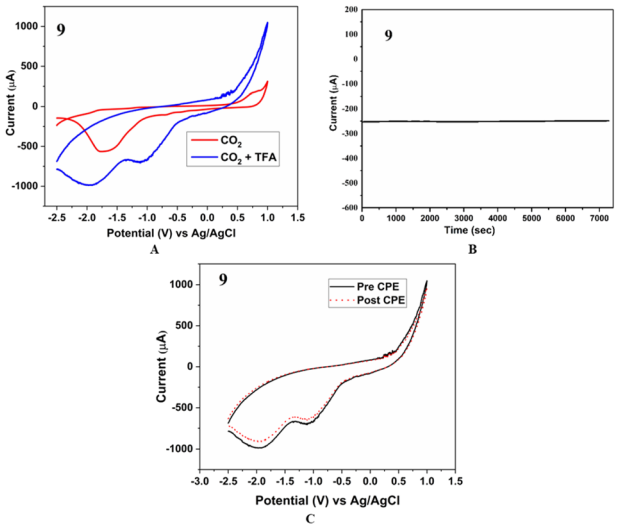

Fig. 4 (A) The cyclic voltammograms of **9** under CO_2 (red line) and TFA (blue line). Experiments were performed at the 100 mV s^{-1} scan rate in DMF and 0.1 M supporting electrolyte ($TBAPF_6$). (B) The controlled potential electrolysis of **9**. (C) The pre- and post-CPE analysis of **9**.

The bulk electrolysis experiment was performed for a period of 7200 s for **9** at a 10 mV more negative potential than the first cathodic wave. Samples were obtained from the H-cell's headspace to characterize the gaseous product. The controlled potential electrolysis yielded 58% CO and 40% H_2. The CPE plot (Fig. 4B) revealed no major fluctuation in the current and proved that the catalyst was robust at 7200 s. The post-CPE cyclic voltammetry measurements were also performed and revealed no characteristic change in the respective reduction and oxidation peaks (Fig. 4C).

The best catalyst **9** in this work was compared with several other palladium complexes reported in the literature, and was found to be superior in terms of the catalytic efficiency parameters. Therrien's Pd–NHC pincer complex showed a maximum TOF of 11 s^{-1}, K_{cat} of 30 M^{-1} s^{-1}, and η of −640 mV.[24] Wolf studied the influence of para substituents (OMe, Br, COOR) in a series of palladium–NHC complexes with general the formula [Pd(C^N^C)Cl]OTf on CO_2 reduction catalysis[27] and showed TOFs in the range of 1–9 s^{-1}.

A mechanism for the conversion of CO_2 into CO and H_2 is proposed based on the literature[25] and is shown in Scheme 4. The catalyst [PYA-Pd(II)–Cl]Cl generated [PYA-Pd(0)] species after the addition of two electrons *via* electroreduction from an external source. Depending on the favorable kinetics, two pathways are suggested. In the first case, the interaction of CO_2 with the reduced catalyst species produces a metal–carboxylate intermediate, [PYA-Pd(II)–CO_2^-], that upon protonation with TFA results in the formation of CO. In the other case, the proton adds to the electron-rich [PYA-Pd(0)] and generates the hydride intermediate, [PYA-Pd(II)–H], that reacts with the next proton and generates hydrogen gas. It was noticed that with the addition of acid from 10 mmol to 40 mmol, the cathodic current increased but the ratio of CO to H_2 remained unaffected.

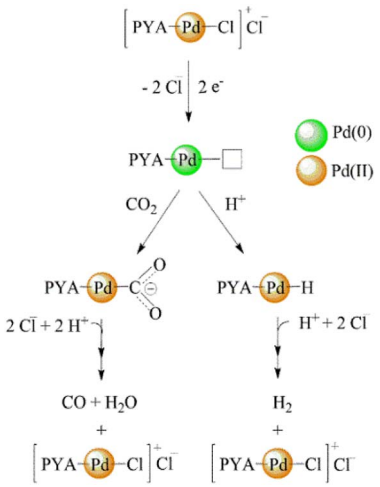

Scheme 4 The proposed mechanism of CO and H_2 selectivity in PYA-Pd complexes.

However, upon the addition of 50 mmol concentration of the TFA, hydrogen production was increased to 47% while the CO was decreased to 50%. At the same time, the overpotential moved to 20 mV more positive potential (Fig. S16†).

To rule out the idea that the high activity and selectivity of **9** were due to elemental palladium deposited from considerable Pd demetallation, a "rinse test" was carried out. To get rid of any loosely bound molecular Pd catalyst, the working electrode from the CPE experiments with **9** was gently rinsed twice with DMF after immersion overnight in DMF. The electrode was then tested to see if Pd metal had been plated onto the carbon electrode during the earlier experiment using a brand-new, catalyst-free electrolyte solution. The little CO generation and negligible current enhancements proved that the electrode was devoid of heterogenized Pd catalyst or elemental palladium.

3 Experimental section

3.1 General consideration

A typical Schlenk line apparatus was used for the synthesis of the proligand, ligands, and the respective palladium(II) complexes. The chemical reagents and solvents were used with or without additional purification or drying depending on the conditions. Analytical grade *N*,*N*-dimethylformamide (DMF), acetonitrile, acetone, dichloromethane, and diethyl ether were purchased from DaeJung, Korea, and were dried and stored over molecular sieves in Schlenk flasks before use. Triethylamine, pyridine-2,6-dicarboxylic acid, 4-aminopyridine, and triphenylphosphite were purchased from Merck Chemicals. Tetrabutylammonium hexafluorophosphate, iodoethane, 1-bromobutane, and benzyl chloride were acquired from Sigma Aldrich. Palladium(II) acetate, and bis(benzonitrile)dichloropalladium were purchased from Aldrich.

^{1}H and ^{13}C NMR spectra were collected using a Bruker AV300 spectrometer. The Campbell Microanalytical Laboratory at the University of Otago collected the elemental analysis data of the samples for C, H, N analysis. IR data of the compounds were obtained from Thermo Scientific Nicolet-6700 FT-IR (4000–400 cm^{-1}). A UVGL-58 UV lamp was used to monitor the reactions using TLC plates. The melting points of all the compounds were measured on a Sanyo Gallen Kamp MPD350 instrument. Electrochemical studies were performed on a CH-I760 electrochemical workstation.

3.2 Electrochemistry

Electrocatalytic activities were performed by using cyclic voltammetry and controlled potential electrolysis. An air-tight H-shaped electrochemical cell with three conventional electrodes, namely glassy carbon as the working electrode (with an area of 7 mm^2), counterelectrode of Pt mesh, and Ag/AgCl (Ag wire dipped in 3.5 M KCl solution isolated from the bulk solution by a Vycor frit) as the reference electrode. An H-cell was used to put the working and Pt mesh counterelectrode in separate compartments and to avoid direct interaction of CO with Pt. Electrochemical studies were performed under inert as well as CO_2 environments. The H-cell was filled with 2 mM solutions of **6–11** along with 0.1 M $TBAPF_6$ (tetrabutylammonium hexafluorophosphate) as the supporting electrolyte in 15 mL of dimethyl formamide in the absence or presence of TFA. Gases were purged for 10 min followed by running the instrument at various scan rates. The glassy carbon electrode was polished with 1, 0.3, and 0.05 μM alumina paste successively followed by sonication for 5 min in distilled water followed by methanol. It was finally rinsed with distilled water before each experiment. The glassy carbon electrodes were eviscerated by electrochemical oxidation at +1.0 V *versus* Ag/AgCl followed by a thorough rinsing with methanol and acetone. Electrolyte solutions of 0.1 M $TBAPF_6$ in anhydrous DMF with and without catalysts were sparged with N_2 and CO_2 for 15–20 min prior to each experiment. The sparging of CO_2 for 20 min was enough to create a concentration of CO_2 ~0.18 M in DMF.[24] The precursor N^2,N^6-di(pyridin-4-yl)pyridine-2,6-dicarboxamide (**1**) was prepared following the reported method.[33]

3.3 General procedure for the synthesis of proligands (2–4)

Precursor (**1**) and respective alkyl halide were charged to an evacuated 100 mL round-bottom two-neck flask. Acetonitrile was added and the reaction mixture was refluxed at 80 °C for an appropriate time. The reaction mixture was cooled to room temperature and the precipitates were collected (*via* filtration), washed with acetone and diethyl ether, and dried *in vacuo* to yield pure products.

3.3.1 4,4′-((Pyridine-2,6-dicarbonyl)bis(azanediyl))bis(1-ethylpyridin-1-ium)chloride, (H_2L_{Et}) (2). Quantities used were: **1** (400 mg, 1.25 mmol, 1.00 eq.), ethyl iodide (0.5 mL, 973 μmol, 5.00 eq.), acetonitrile (25 mL). Reaction time: refluxed for 10 h.

Yield: 90%. Color: yellow. mp: 230 °C. Anal. calculated for $C_{21}H_{23}I_2N_2O_5$: C, 66.83; H, 6.14; N, 18.55. Found: C, 66.60; H, 6.34; N, 18.28. IR (KBr, cm^{-1}): 3425 (NH), 3005 (Ar-CH), 2970, 2872 (Aliph-CH), 1668 (C=O), 1620 (C=N), 1226 (C–N). ^{1}H NMR δ (ppm)/J (Hz)/DMSO-d_6/300 MHz: 11.97 (s, 2H, H^{NH}), 9.02 (d, J = 7.2, 4H, H^{Ar}), 8.59–8.47 (m, 5H, H^{Ar}), 4.59–4.52 (m, 4H,

H^{CH_2}), 1.58 (t, J = 15, 6H, H^{CH_3}). ^{13}C NMR δ (ppm)/DMSO-d_6/75 MHz: 163.7(Ar–C=O), 151.5, 147.6, 145.5, 141.5, 127.8, 116.7 (Ar), 55.4 (CCH_2), 16.5 (CCH_3).

3.3.2 4,4′-((Pyridine-2,6-dicarbonyl)bis(azanediyl))bis(1-butylpyridin-1-ium)bromide, (H_2L_{Bu}) (3). Quantities used were: **1** (500 mg, 1.56 mmol, 1.00 eq.), butyl bromide (1.69 mL, 2.15 mmol, 10.00 eq.), acetonitrile (40 mL). Reaction time: refluxed for 50 h.

Yield: 90%. Color: white. mp: 238 °C. Anal. calcd for $C_{25}H_{31}Br_2N_5O_2$: C, 50.61; H, 5.27; N, 11.80. Found: C, 50.46; H, 5.08; N, 11.56. IR (KBr, cm^{-1}): 3431 (NH), 3006 (Ar-CH), 2871 (Aliph-CH), 1692 (C=O), 1638 (C=N), 1227 (C–N). ^{1}H NMR δ (ppm)/J (Hz)/DMSO-d_6/300 MHz: 12.19 (s, 2H, H^{NH}), 9.07 (d, J = 6, 4H, H^{Ar}), 8.69 (d, 4H, J = 7.5, H^{Ar}) 8.56–8.45 (m, 3H, J = 7.8, 6.6, H^{Ar}), 4.54 (pseudo triplet, 4H, H^{CH_2}), 1.90 (pseudo triplet, 4H, H^{CH_2}), 1.33 (pseudo triplet, 4H, H^{CH_2}), 0.96 (pseudo triplet, 6H, H^{CH_3}). ^{13}C NMR δ (ppm)/DMSO-d_6/75 MHz: 164.0 (C=O), 151.7, 147.9, 145.7, 141.3, 128.0, 116.8 (Ar), 59.5, 32.9, 19.2 (CCH_2), 13.8 (CCH_3).

3.3.3 4,4′-((Pyridine-2,6-dicarbonyl)bis(azanediyl))bis(1-benzylpyridin-1-ium)chloride, (H_2L_{Bz}) (4). Quantities used were: **1** (250 mg, 780 μmol, 1.00 eq.), benzyl chloride (3.6 mL, 3.96 mmol, 40.00 eq.), acetonitrile (15 mL). Reaction time: refluxed for 10 h.

Yield: 90%. Color: white. mp: 276 °C. Anal. calcd for $C_{31}H_{27}Cl_2N_5O_2$: C, 74.23; H, 5.43; N, 13.96. Found: C, 74.06; H, 5.15; N, 13.75. IR (KBr, cm^{-1}): 3431 (NH), 3063 (Ar-CH), 2395 (Aliph-CH), 1691 (C=O), 1512 (C=N), 1267 (C–N). ^{1}H NMR δ (ppm)/J (Hz)/DMSO-d_6/300 MHz: 13.20 (s, 2H, H^{NH}), 9.14 (d, J = 7.2, 4H, H^{Ar}), 8.99 (d, J = 7.2, 4H, H^{Ar}) 8.52 (d, J = 8.4, 2H, H^{Ar}) 8.49 (m, 1H, H^{Ar}). 7.54–7.44 (m, 10H, H^{Ar}), 5.77 (s, 4H, H^{CH_2}). ^{13}C NMR δ (ppm)/DMSO-d_6/75 MHz: 164.6 (C=O), 152.9, 148.3, 145.5, 140.9, 135.2, 129.6, 128.9, 128.2, 117.4 (Ar), 62.2(CCH_2).

3.3.4 N^2,N^6-Bis(1-butylpyridin-4(1H)-ylidene)pyridine-2,6-dicarboxamide, (L_{Bu}) (5). (H_2L_{Bu}) (**3**) and 15 mL dichloromethane were placed in 100 mL separating funnel followed by the addition of 2 mol L^{-1} aqueous potassium hydroxide solution. Vigorous shaking resulted in the dissolution of the solid material. The organic layer was separated, and the solvent was reduced by rotary evaporation. White fine precipitates were obtained and dried *in vacuo* to yield the pure product.

Yield: 67%. Color: white. mp: 300 °C. Anal. calcd for $C_{25}H_{29}N_5O_2$: C, 69.58; H, 6.77; N, 16.23. Found: C, 69.35; H, 6.68; N, 16.05. IR (KBr, cm^{-1}): 3053 (Ar-CH), 2930 (Aliph-CH), 1650 (C=O), 1628 (C=N), 1575 (C=C). ^{1}H NMR δ (ppm)/J (Hz)/DMSO-d_6/300 MHz: 8.77 (d, J = 6.9, 4H, H^{Ar}), 8.48 (d, J = 7.8, 1H, H^{Ar}), 8.10 (d, J = 7.8, 2H, H^{Ar}), 7.94 (d, J = 6.9, 4H, H^{Ar}), 4.45 (t, J = 7.2, 4H, H^{CH_2}), 1.89–1.81 (t, J = 9, 4H, H^{CH_2}), 1.32–1.24 (m, 4H, H^{CH_2}), 0.94 (t, J = 6, 6H, H^{CH_3}). ^{13}C NMR δ (ppm)/DMSO-d_6/75 MHz: 170.5 (C=O), 161.5, 149.6, 143.3, 128.3, 125.8(Ar), 59.3, 32.9, 19.2 (CCH_2), 13.8 (CCH_3).

3.4 General procedure for the synthesis of complexes (6–11)

H_2L (1.00 eq.), palladium precursor (1.10 eq.), and acetonitrile (5 mL) were combined in an evacuated 25 mL two-necked round-bottom flask. After stirring for 15 min, DBU or sodium acetate (3.00 eq.) was added, and the reaction mixture was heated under reflux (80 °C) in an atmosphere of dry nitrogen for several hours. The solution was cooled to room temperature and the precipitates formed were filtered and dried *in vacuo* to yield a pure product.

3.4.1 Complex 6, [Pd(L_{Et})(OAc)][OAc]. Quantities used were: **2** (100 mg, 158 μmol), palladium acetate (64 mg, 174 μmol), DBU (71 μL, 474 μmol). Reflux time: 2 h.

Yield 67%. Color: brown. mp: 254 °C. Anal. calcd for $C_{25}H_{27}N_5O_6Pd$: C, 50.05; H, 4.54; N, 11.67. Found: C, 50.31; H, 4.30; N, 11.54. IR (KBr, cm^{-1}): 3072 (Ar-CH), 2900 (Aliph-CH), 1650 (C=O), 1618 (OCH_3,C=O), 1556 (C=N), 1558 (C=C). ^{1}H NMR δ (ppm)/J (Hz)/DMSO-d_6/300 MHz: 8.75 (d, J = 6.9, 4H, H^{Ar}), 8.46 (t, J = 7.8, 1H, H^{Ar}), 8.07 (d, J = 7.8, 2H, H^{Ar}), 7.89 (d, J = 6.9, 4H, H^{Ar}), 4.46 (q, J = 7.2, 4H, H^{CH_2}), 1.62 (s, 3H, H^{OCH_3}), 1.51 (t, 6H, H^{CH_3}). ^{13}C NMR δ (ppm)/DMSO-d_6/75 MHz: 175.8 (OCH_3,C=O), 170.3 (C=O), 161.7, 150.4, 143.3, 142.8, 128.3, 123.0 (Ar), 54.8 (CCH_2), 24.8 (OCH_3), 16.6 (CCH_3).

3.4.2 Complex 7, [Pd(L_{Bu})(OAc)][OAc]. Quantities used were: **3** (50 mg, 84 μmol), palladium(II) acetate (21 mg, 93 μmol), sodium acetate (22 mg, 253 μmol). Reflux time: 3 h.

Yield: 67%. Color: orange-yellow. mp: 300 °C. Anal. calcd for $C_{29}H_{35}N_5O_6Pd$: C, 50.09; H, 5.38; N, 10.68. Found: C, 50.38; H, 5.50; N, 10.45. IR (KBr, cm^{-1}): 3044 (A-CH), 2930 (Aliph-CH), 1645 (C=O), 1612 (OCH_3,C=O), 1598 (C=N),1556 (C=C). ^{1}H NMR δ (ppm)/J (Hz)/DMSO-d_6/300 MHz: 8.78 (d, J = 6.3, 4H, H^{Ar}), 8.49 (t, J = 8.7, 1H, H^{Ar}), 8.09 (d, J = 7.5, 2H, H^{Ar}), 7.90 (d, J = 5.7, 4H, H^{Ar}), 4.44 (pseudo triplet, 4H, H^{CH_2}), 1.85 (pseudo triplet, J = 7.5, 4H, H^{CH_2}), 1.59 (s, 3H, H^{OCH_3}), 1.28 (q, J = 7.2, 4H, H^{CH_2}), 0.93 (pseudo triplet, J = 6.9, 6H, H^{CH_3}). ^{13}C NMR δ (ppm)/DMSO-d_6/75 MHz: 170.4 (OCH_3,C=O), 162.0 (C=O), 149.4, 143.3, 128.3, 126.6 (Ar), 59.3 (CCH_2), 32.9 (CCH_2), 19.2 (OCH_3), 13.8 (CCH_3).

3.4.3 Complex 8, [Pd(L_{Bz})(OAc)][OAc]. Quantities used were: **4** (100 mg, 175 μmol), palladium(II) acetate (43 mg, 193 μmol), DBU (80 μL, 525 mmol). Reflux time: 2 h.

Yield 68%. Color: olive-green. mp: 282 °C. Anal. calcd for $C_{35}H_{31}N_5O_6Pd$: C, 58.06; H, 4.32; N, 9.67. Found: C, 58.30; H, 4.58; N, 9.45. IR (KBr, cm^{-1}): 3016 (Ar-CH), 2926 (Aliph-CH), 1653 (C=O), 1621 (OCH_3,C=O), 1600 (C=N), 1575 (C=C). ^{1}H NMR δ (ppm)/J (Hz)/DMSO-d_6/300 MHz: 8.90 (d, J = 6.9, 4H, H^{Ar}), 8.41 (t, J = 7.8, 1H, H^{Ar}), 8.04 (d, J = 7.8, 2H, H^{Ar}), 7.90 (d, J = 6.6, 4H, H^{Ar}), 7.47–7.41 (m, J = 3.6, 10H, H^{Ar}), 5.67 (s, 4H, H^{CH_2}), 1.50 (s, 3H, H^{OCH_3}). ^{13}C NMR δ (ppm)/DMSO-d_6/75 MHz: 170.3(OCH_3, C=O), 162.1 (C=O), 149.4, 143.7, 142.8, 135.5, 129.6, 129.5, 128.8, 128.4, 123.2 (Ar), 61.8 (CCH_2), 24.7 (OCH_3).

3.4.4 Complex 9, [Pd(L_{Et})(Cl)][Cl]. Quantities used were: **2** (100 mg, 158 μmol), bis(benzonitrile)dichloropalladium (61 mg, 158 μmol). DBU (75 μL, 480 μmol). Reflux time: 70 min.

Yield: 90%. Color: dark green. mp: 280 °C. Anal. calcd for $C_{21}H_{21}Cl_2N_5O_2Pd$: C, 45.63; H, 3.83; N, 12.67. Found: C, 45.88; H, 3.60; N, 12.45. IR (KBr, cm^{-1}): 3170 (Ar-CH), 2912,2871 (Aliph-CH), 1692 (C=O), 1492 (C=C), 1227 (C–N). ^{1}H NMR δ (ppm)/J (Hz)/DMSO-d_6/300 MHz: 8.76 (d, J = 6.2, 4H, H^{Ar}), 8.46 (dd, 1H, J = 7.8, H^{Ar}), 8.08 (d, J = 0.9, 2H, H^{Ar}), 7.95 (d, J = 6.6, 4H, H^{Ar}), 4.48 (m, 4H, H^{CH_2}), 1.52 (t, J = 6, 6H, H^{CH_3}). ^{13}C NMR δ (ppm)/DMSO-d_6/75 MHz: 170.5 (C=O), 161.5, 149.7, 143.0, 142.7, 128.3, 125.7 (Ar), 55.0 (CCH_2), 16.5 (CCH_3).

3.4.5 Complex 10, [Pd(L_{Bu})(Cl)][Cl]. Quantities used were: **3** (100 mg, 160 μmol), bis(benzonitrile)dichloropalladium (64 mg, 160 μmol), DBU (75 μL, 480 μmol). Reflux time: 70 min.

Yield: 60%. Color: yellowish green. mp: 295 °C. Anal. calcd for $C_{25}H_{29}Cl_2N_5O_2Pd$: C, 49.32; H, 4.80; N, 11.50. Found: C, 49.64; H, 4.57; N, 11.73. IR (KBr, cm^{-1}): 3006 (Ar-CH), 2871 (Aliph-CH), 1682 (C=O), 1517 (C=N), 1455 (C=C), 1376 (C–N). ^{1}H NMR δ (ppm)/J (Hz)/DMSO-d_6/300 MHz: 8.77 (pseudo triplet, 4H, H^{Ar}), 8.44 (pseudo triplet, 1H, H^{Ar}), 8.08–7.94 (m, 6H, H^{Ar}) 4.43 (pseudo triplet, 4H, H^{CH_2}), 1.86–1.64 (m, 4H, H^{CH_2}), 1.28 (pseudo triplet, 4H, H^{CH_2}), 0.91 (pseudo triplet, 6H, H^{CH_3}). ^{13}C NMR δ (ppm)/DMSO-d_6/75 MHz: 170.5 (C=O), 161.5, 149.6, 143.8, 143.3, 128.3, 125.7 (Ar), 59.2, 32.9, 19.2 (CCH_2), 13.8 (CCH_3).

3.4.6 Complex 11, [Pd(L_{Bz})(Cl)][Cl]. Quantities used were: **4** (250 mg, 436 μmol), bis(benzonitrile)dichloropalladium (167 mg, 436 μmol), DBU (200 μL, 1.30 mmol). Reflux time: 60 min.

Yield: 75%. Color: yellow. mp: 254 °C. Anal. calcd for $C_{31}H_{25}Cl_2N_5O_2Pd$: C, 55.01; H, 3.72; N, 10.35. Found: C, 55.25; H, 3.55; N, 10.13. IR (KBr, cm^{-1}): 3058 (Ar-CH), 2994 (Aliph-CH), 1658 (C=O), 1644 (C=N), 1351 (C–N). ^{1}H NMR δ (ppm)/J (Hz)/DMSO-d_6/300 MHz: 8.90 (d, $J = 6.9$, 4H, H^{Ar}), 8.46 (t, $J = 7.8$, 1H, H^{Ar}), 8.08 (d, $J = 6.9$, 2H, H^{Ar}), 7.96 (d, $J = 6$, 3H, H^{Ar}), 7.53–7.40 (m, $J = 15$, 11H, H^{Ar}), 5.68 (s, 4H, H^{CH_2}). ^{13}C NMR δ (ppm)/DMSO-d_6/75 MHz: 170.5 (C=O), 161.8, 149.6, 143.4, 135.3, 129.6, 129.0, 128.4, 128.1, 125.9 (Ar), 62.0 (CCH_2).

4 Conclusion

New *N*,*N*,*N* pincer complexes of palladium were synthesized and successfully characterized. The donor-flexible nature of the pyridylidene amide (PYA) spectator ligands with their X and L type limiting resonance structures were effectively exploited to facilitate palladium-catalyzed CO_2 reduction reactions. The synergy of palladium with PYA bearing ethylated groups and chloride being a better labile ligand activated CO_2 the most compared to the respective benzyl and butyl PYA analogues and acetate actor ligand. A minimum overpotential of 0.40 V and a maximum turnover frequency (TOF) of 101 s^{-1} with a 58% FE of CO was calculated for **9** under electrocatalytic conditions in TFA.

Author contributions

Afshan Khurshid: investigation, visualization, writing – original draft, data curation, validation. Tania Tanveer: formal analysis, investigation, visualization, writing – original draft, data curation. Komal Hafeez: formal analysis, investigation, visualization, data curation. Maqsood Ahmed: single-crystal analysis. Zareen Akhter: resources. Muhammad Naveed Zafar: conceptualization, methodology, writing – review & editing, resources, project administration, funding acquisition, supervision.

Conflicts of interest

There are no conflicts to declare.

Acknowledgements

We are highly grateful to Higher education commission (HEC) Pakistan for providing research grant to principal investigator (M. N. Z).

References

1 E. E. Benson, C. P. Kubiak, A. J. Sathrum and J. M. Smieja, *Chem. Soc. Rev.*, 2009, **38**, 89–99.
2 M. Mikkelsen, M. Jørgensen and F. C. Krebs, *Energy Environ. Sci.*, 2010, **3**, 43–81.
3 S. Slater and J. H. Wagenknecht, *J. Am. Chem. Soc.*, 1984, **106**, 5367–5368.
4 M. Rakowski Dubois and D. L. Dubois, *Acc. Chem. Res.*, 2009, **42**, 1974–1982.
5 D. L. DuBois, A. Miedaner and R. C. Haltiwanger, *J. Am. Chem. Soc.*, 1991, **113**, 8753–8764.
6 D. L. DuBois and A. Miedaner, *J. Am. Chem. Soc.*, 1987, **109**, 113–117.
7 B. D. Steffey, C. J. Curtis and D. L. DuBois, *Organometallics*, 1995, **14**, 4937–4943.
8 A. Miedaner, B. C. Noll and D. L. DuBois, *Organometallics*, 1997, **16**, 5779–5791.
9 A. M. Hossain, T. Nagaoka and K. Ogura, *Electrochim. Acta*, 1996, **41**, 2773–2780.
10 A. M. Hossain, T. Nagaoka and K. Ogura, *Electrochim. Acta*, 1997, **42**, 2577–2585.
11 J. v. Vlugt and J. Reek, *Angew Chem. Int. Ed. Engl.*, 2009, **48**, 8832–8846.
12 T. K. Michaelos, D. Y. Shopov, S. B. Sinha, L. S. Sharninghausen, K. J. Fisher, H. M. Lant, R. H. Crabtree and G. W. Brudvig, *Acc. Chem. Res.*, 2017, **50**, 952–959.
13 J. A. Wright, A. A. Danopoulos, W. B. Motherwell, R. J. Carroll and S. Ellwood, *J. Organomet. Chem.*, 2006, **691**, 5204–5210.
14 C. Arana, S. Yan, K. M. Keshavarz, K. T. Potts and H. D. Abruna, *Inorg. Chem.*, 1992, **31**, 3680–3682.
15 G. Chiericato Jr, C. Arana, C. Casado, I. Cuadrado and H. Abruna, *Inorg. Chim. Acta*, 2000, **300**, 32–42.
16 F. W. Liu, J. Bi, Y. Sun, S. Luo and P. Kang, *ChemSusChem*, 2018, **11**, 1656–1663.
17 N. Elgrishi, M. B. Chambers, V. Artero and M. Fontecave, *Phys. Chem. Chem. Phys.*, 2014, **16**, 13635–13644.
18 N. Elgrishi, M. B. Chambers and M. Fontecave, *Chem. Sci.*, 2015, **6**, 2522–2531.
19 K. Talukdar, A. Issa and J. W. Jurss, *Front. Chem.*, 2019, **7**, 330.
20 G. K. Rao, W. Pell, I. Korobkov and D. Richeson, *Chem. Commun.*, 2016, **52**, 8010–8013.
21 J. D. Cope, N. P. Liyanage, P. J. Kelley, J. A. Denny, E. J. Valente, C. E. Webster, J. H. Delcamp and T. K. Hollis, *Chem. Commun.*, 2017, **53**, 9442–9445.
22 M. Sheng, N. Jiang, S. Gustafson, B. You, D. H. Ess and Y. Sun, *Dalton Trans.*, 2015, **44**, 16247–16250.
23 T. H. Myren, A. M. Lilio, C. G. Huntzinger, J. W. Horstman, T. A. Stinson, T. Franklin, C. Moore, B. Lama, H. H. Funke and O. R. Luca, *Organometallics*, 2018, **38**, 1248–1253.

24 J. A. Therrien, M. O. Wolf and B. O. Patrick, *Inorg. Chem.*, 2014, **53**, 12962–12972.
25 E. E. DeLuca, Z. Xu, J. Lam and M. O. Wolf, *Organometallics*, 2018, **38**, 1330–1343.
26 J. Therrien, M. Wolf and B. Patrick, *Dalton Trans.*, 2018, **47**, 1827–1840.
27 J. A. Therrien and M. O. Wolf, *Inorg. Chem.*, 2017, **56**, 1161–1172.
28 J. A. Therrien, M. O. Wolf and B. O. Patrick, *Inorg. Chem.*, 2015, **54**, 11721–11732.
29 J. Chang, J.-X. Mao, M. Ding, J. Zhang and X. Chen, *Inorg. Chem.*, 2023, **62**, 4971–4979.
30 P. D. Boyd, L. J. Wright and M. N. Zafar, *Inorg. Chem.*, 2011, **50**, 10522–10524.
31 M. N. Zafar, S. Masood, T. S. T. Muhammad, A. F. Dalebrook, M. F. Nazar, F. P. Malik, E. U. Mughal and L. J. Wright, *Dalton Trans.*, 2019, **48**, 15408–15418.
32 M. Zafar, Development of New ligands for homogeneous Transition metal catalysts, *PhD dissertation*, University of Aukland, New Zealand, 2011.
33 A. Dorazco-González, H. Höpfl, F. Medrano and A. K. Yatsimirsky, *J. Org. Chem.*, 2010, **75**, 2259–2273.
34 D. L. Pavia, G. M. Lampman, G. S. Kriz, J. Vyvyan and A. López Maestresalas, *Introduction to Spectroscopy*, 2008, vol. 153, p. 752.
35 I. Georgieva, N. Mintcheva, N. Trendafilova and M. Mitewa, *Vib. Spectrosc.*, 2001, **27**, 153–164.
36 P. Zanello, C. Nervi and F. F. De Biani, *Inorganic Electrochemistry: Theory, Practice and Application*, Royal Society of Chemistry, 2019.
37 J.-M. Savéant, *Elements of Molecular and Biomolecular Electrochemistry: An Electrochemical Approach to Electron Transfer Chemistry*, John Wiley & Sons, 2006.
38 R. S. Nicholson and I. Shain, *Anal. Chem.*, 1964, **36**, 706–723.
39 C. W. Machan, M. D. Sampson and C. P. Kubiak, *J. Am. Chem. Soc.*, 2015, **137**, 8564–8571.